

1
2
3
4
5
6
7
8
9
10
11
12
13
14
15
16
17
18
19

Rhythmic variations in prefrontal inter-neuronal correlations, their underlying mechanisms and their behavioral correlates

Ben Hadj Hassen*¹, S., Gaillard*¹, C., Astrand^{1,2}, E., Wardak^{1,3}, C., Ben Hamed¹, S.

*. These two authors contributed equally to this work

1. Institut des Sciences Cognitives Marc Jeannerod, CNRS, UMR5229, 67 Boulevard Pinel, 69675 Bron Cedex, France

2. Mälardalen University, IDT, Högskoleplan 1, 721 23 Västerås, Sweden

3. Imagerie et Cerveau (iBrain), 10 Boulevard Tonnellé 37032 Tours Cedex 1, France

Lead contact: Suliann Ben Hamed, benhamed@isc.cnrs.fr

Corresponding author: Suliann Ben Hamed, benhamed@isc.cnrs.fr; Sameh Ben Hadj Hassen, sameh.ben-hadj@isc.cnrs.fr

Key words: noise correlation, Spike-LFP coherence, Phase locking, prefrontal cortex, alpha, beta, rhythmic cognition.

20 **Summary**

21 Functional neuronal correlations between pairs of neurons are thought to play an important role
22 in neuronal information processing and optimal neuronal computations during attention,
23 perception, decision-making and learning. These noise correlations are often assumed to be
24 stable in time. However, recent studies suggest that cognitive processes are rhythmic, this
25 rhythmicity accounting for variations in overt behavioral performance. Whether this
26 rhythmicity coincides with variations in shared noise variability is unknown. Here, we perform
27 simultaneous recordings from the macaque frontal eye fields, while animals are engaged in a
28 spatial memory task. We report that noise correlations in prefrontal cortex fluctuate
29 rhythmically in the high alpha (10-16Hz) and beta (20-30Hz) frequency ranges. Importantly,
30 these rhythmic modulations in shared neuronal variability account for dynamic changes in overt
31 behavioral performance. They also coincide with increased spike-LFP phase coupling in these
32 specific frequency ranges, the spatial profile of which vary between superficial and deep
33 cortical layers. Finally, we demonstrate, using an artificial neuronal model, that rhythmic
34 variations in noise correlation oscillations parsimoniously arise from long range (LFP) and local
35 spike-LFP phase coupling mechanisms. Thus a significant portion of noise correlation
36 fluctuations can be attributed to long-range global network rhythmicity.

37

38 **Introduction**

39 Neuronal responses to the same stimulus fluctuate in time and across repetitions^{1,2}. This
40 response variability is thought to be shared among functionally close neurons and is often
41 referred to as noise correlations³. These noise correlations reflect the amount of co-variability,
42 in the trial-to-trial fluctuations in the response of pairs of neurons, to repeated presentations of
43 identical stimuli, or under identical behavioral conditions, in the absence of any sensory
44 stimulation. However, the exact origin of this shared neuronal variability remains unclear. It
45 has been proposed that it arises from shared connectivity⁴, global fluctuations in the excitability
46 of cortical circuits^{5,6}, feedback signals⁷, internal areal dynamics⁸⁻¹⁰, as well as bottom-up
47 peripheral sensory processing¹¹.

48 In fact, noise correlations have received a lot of attention and have been measured in a
49 variety of brains areas, under numerous behavioral and stimulus conditions. Several studies
50 suggest that noise correlations have a critical impact on cortical signal processing as well as
51 onto behavioral performance^{3,11,11-14}, with learning or changes in behavioral state and attention
52 ^{2,15-23}.

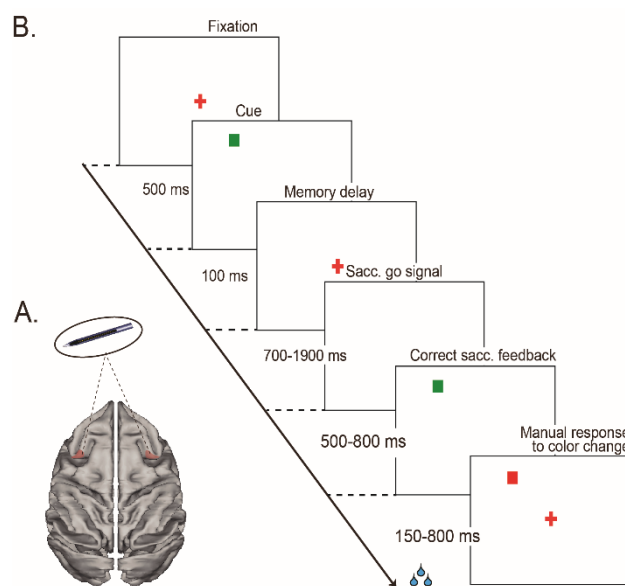
53 The majority of these studies have measured how noise correlations are affected by
54 spatial attention orientation, assuming stability in time. However, recent studies suggest that
55 cognitive processes are based on rhythmic mechanisms that take place in the theta and alpha
56 frequency ranges. This rhythmicity accounts for variations in overt behavioral performance
57 ^{24,25}. Whether this rhythmicity coincides with variations in shared noise variability is unknown.
58 ²⁶ describe variations in shared noise variability in the gamma band. Here, we demonstrate
59 variations in prefrontal noise correlations in the alpha and beta frequency ranges. To achieve
60 this, we recorded neuronal responses from macaque frontal eye fields (FEF), a cortical region
61 at the source of spatial attention control signals²⁷⁻³⁰ and in which noise correlations have been
62 shown to vary as a function of spatial attention¹⁵ and spatial memory^{31,32}. Monkeys were
63 engaged in a spatial memory task. Overall, we demonstrate for the first time, rhythmic
64 modulations of prefrontal noise correlations in two specific functional frequency ranges: the
65 high alpha (10-16Hz) and the beta (20-30Hz) frequency ranges. Crucially, we show that these
66 rhythmic modulations in noise correlations account both for overt behavioral performance and
67 for layer specific modulations in spike-field phase coupling. Based on an artificial model, we
68 demonstrate that rhythmic variations in noise correlation oscillations parsimoniously arise from
69 long range (LFP) and local spike-LFP phase coupling mechanisms.

70

71 Results

72 Neuronal recordings were performed in the prefrontal cortex, specifically in the frontal
73 eye field (FEF, figure 1A), a structure known to play a key role in covert spatial attention^{28,33–}
74³⁵. In each session, multi-unit activity (MUA) and local field potential (LFP) were recorded
75 bilaterally, while monkeys performed a memory guided saccade task (figure 1B). Specifically,
76 monkeys were required to hold the position of a spatial cue in memory for 700 to 1900ms and
77 to perform a saccade towards the memorized spatial location on the extinction of the fixation
78 point that served as a go signal. In the following, noise correlations between the different
79 prefrontal signals of the same hemisphere were computed during the time interval running from
80 300ms to 1500ms following cue offset, on neuronal activities averaged over 200ms sliding
81 windows (step of 10ms). As shown by previous studies, noise correlations decrease as a
82 function of cortical distance (Figure S1A, 1-way ANOVA, $p < 0.001$, Wilcoxon rank sum test,
83 $p < 0.001$ for 750 μm , $p < 0.001$ for 1000 μm ,^{23,36,37} and are significantly lower among neuronal
84 pairs with different spatial selectivity than neuronal pairs with the same spatial selectivity
85 (Figure S1B, 1-way ANOVA, $p < 0.001$)³⁸.

86



87

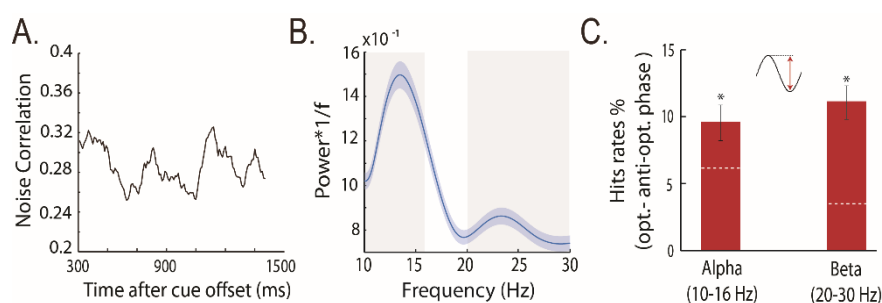
88 **Figure 1: (A) Recordings sites.** On each session, 24-contact recording probes were
89 placed in the left and right FEFs. **(B) Memory-guided saccade task.** Monkeys had
90 to fixate a red central cross. A visual cue was briefly flashed in one of four possible
91 locations on the screen. Monkeys were required to hold fixation until the fixation
92 cross disappeared and then produce a saccade to the spatial location indicated by
93 the cue fixation point offset. On success, the cue re-appeared and the monkeys had

94 to fixate it. They were then rewarded for producing a manual response 150ms to
95 800ms following the color change of this new fixation stimulus.

96 *Rhythmic fluctuations in noise correlations modulate behavioral response*

97 Very few studies have addressed the question of how noise correlations vary as a
98 function of time. ²⁶ show that in primary visual cortex V1, noise correlations between neurons
99 are modulated by gamma phase, synchronization in the 35-60Hz gamma-band producing
100 maximal stimulus selectivity as well as minimal noise correlations. Whether this generalizes to
101 other cortical regions and whether these variations in noise correlations are of behavioral
102 relevance is currently unknown.

103 Here, we quantify variations in noise correlations during the cue to saccade go signal
104 epoch, away from the initial sensory processing of the spatial cue. Specifically, in each session
105 (n=26), noise correlations were computed between each pair of task-responsive channels
106 (n=671, see Methods), during the spatial memory delay, running from 300ms to 1500ms
107 following cue offset. During this epoch monkeys were required to memorize the cue location
108 and get prepared to produce a spatially oriented saccade in response to an unexpected saccade
109 go signal (fixation cross offset). In these computations, we included only trials with cue to go
110 signal duration longer than 1500ms. Figure 2A shows clear noise correlation fluctuations in
111 time during a representative recording session. Across all session, noise correlations were
112 characterized, during the spatial memory delay, by rhythmic fluctuations taking place in two
113 distinct frequency ranges: a high alpha frequency range (10-16 Hz) and a beta frequency range
114 (20-30Hz), as quantified by a wavelet analysis (figure 2B). Overall, this indicates that noise
115 correlations are rhythmic, their oscillatory pattern being probably reset by cue presentation as
116 has been shown for other types of neuronal oscillatory patterns; ^{25,39-43}.



117
118 **Figure 2: *Rhythmic fluctuations in noise correlations modulate behavioral***
119 ***response***. (A) Single memory guided saccade session example of noise correlation
120 variations as a function of trial time. (B) 1/f weighted power frequency spectra of
121 noise correlation in time (mean +/- s.e.), calculated from 300ms to 1500ms
122 following cue offset. (C) Hit rate modulation by alpha and beta noise correlation at

123 optimal phase as compared to anti-optimal phase, average +/- s.e., dashed white
124 lines represent the 95% confidence interval under the assumption of absence of
125 behavioral performance phase dependence.

126 An important question is whether these rhythmic variations in noise correlations
127 contribute to task-related information processing and account for variations in overt behavioral
128 performance. Indeed, low noise correlation neuronal population states are found to correlate
129 with high neuronal population informational content ³ as well as with high behavioral
130 performance states, i.e. correct trials as compared to incorrect trials ⁴⁴. Here, we show that overt
131 behavioral performance; defined as the proportion of correct trials as compared to misses trials,
132 vary as a function of alpha and beta noise correlation oscillations. Specifically, on a session by
133 session basis, we identify an optimal alpha (10-16Hz) phase for which the behavioral
134 performance is maximal (+9.5%) compared to the corresponding anti-phase for which the
135 behavioral performance is lowest (figure 2C). Similarly, an optimal beta (20-30Hz) phase is
136 found to modulate behavioral performance in the same range of amplitudes (+11%). Overall,
137 we thus demonstrate that the phases of alpha and beta oscillations in prefrontal noise
138 correlations are predictive of overt behavioral performance.

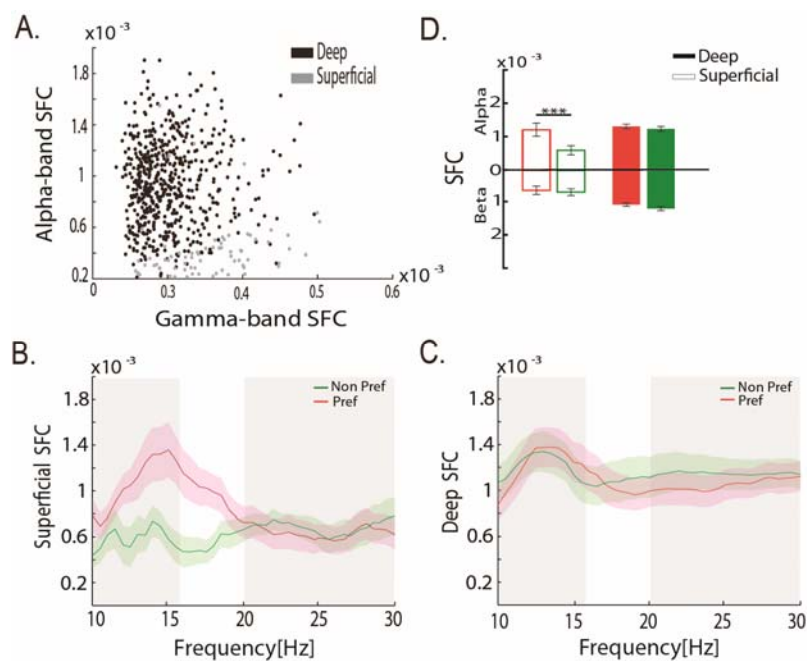
139 ***Oscillations in noise correlations coincide with enhanced spike-LFP phase coupling***
140 ***(SFC) in specific frequency ranges***

141 High alpha and beta oscillations in the local field potentials (LFP) are ubiquitous and
142 are considered to reflect long-range processes. Beta oscillations have been associated with
143 cognitive control and cognitive flexibility. On the other hand, alpha oscillations are associated
144 with attention, anticipation ^{45,46}, perception ⁴⁷⁻⁴⁹, and working memory ⁵⁰. A parsimonious
145 hypothesis is thus that oscillations in noise correlations also arise from long-range process, via
146 specific SFC mechanisms. Confirming this hypothesis, figure S2 represents SFC (as assessed
147 from a PPC analysis, see Materials and Methods), computed during a 1200ms time interval over
148 the spatial memory delay, running from 300ms to 1500ms following cue offset. Spike-LFP
149 phase coupling peaks at the same frequency ranges identified in the noise correlation spectra,
150 namely the high alpha range (10-16Hz) and the beta range (20-30Hz). When considering SFC
151 independently of cortical layer organization, no difference in SFC is found between preferred
152 and non-preferred positions in either frequency ranges. Interestingly, these selective SFC
153 mechanisms are independent from overall LFP power content. Indeed, LFP power on the same
154 dataset shows a deviation from the 1/f expect drop in a broad frequency range running from 15-
155 30 Hz (figure S3A). This increase in LFP power is higher after cue presentation as compared

156 to before (figure S3B). In contrast with SFC, this increase in LFP power is also more
157 pronounced when the monkey is being cued towards the preferred than towards the non-
158 preferred spatial location of the recorded signals (figure S3B). Overall, this thus suggests that
159 oscillations in noise correlations arise from specific phase coupling mechanisms between long-
160 range incoming LFP signals and local spiking mechanisms, independently from phase-
161 amplitude coupling mechanisms.

162 *Spike-LFP phase coupling (SFC) differs between superficial and deep FEF layers*

163 FEF neurons are characterized by a strong visual, saccadic, spatial memory and spatial
164 attention selectivity^{27,28,51}. Previous studies have shown that pure visual neurons are
165 predominantly located in the supragranular layers of the FEF while visuo-motor neurons are
166 predominantly located in its infragranular layers⁵¹⁻⁵⁶.⁵⁷ further show that supragranular FEF
167 neurons predominantly project to striate visual cortex while infragranular FEF neurons
168 predominantly project to the superior colliculus⁵⁸⁻⁶⁰. The question we address here is whether
169 the specific phase coupling mechanisms identified in the previous section are common to both
170 supra- and infragranular FEF layers. Buffalo et al. have shown that, in extra-striate area V4, the
171 ratio between the alpha and gamma spike field coherence discriminate between LFP signals in
172 deep (low alpha / gamma spike field coherence ratio) and superficial cortical layers (high alpha
173 / gamma spike field coherence ratio,⁶¹. In our own data, as recordings were performed
174 tangentially to FEF cortical surface, we have no direct assignation of the recorded MUAs to
175 either superficial or deep cortical layers. However, the LFP alpha / gamma spike field coherence
176 ratio provides a very reliable segregation of visual and visuo-motor MUAs at the same
177 recording sites (figure 3A). We thus consider that, as has been described for area V4, this
178 measure allows for a reliable delineation of superficial and deep layers in area FEF.



179

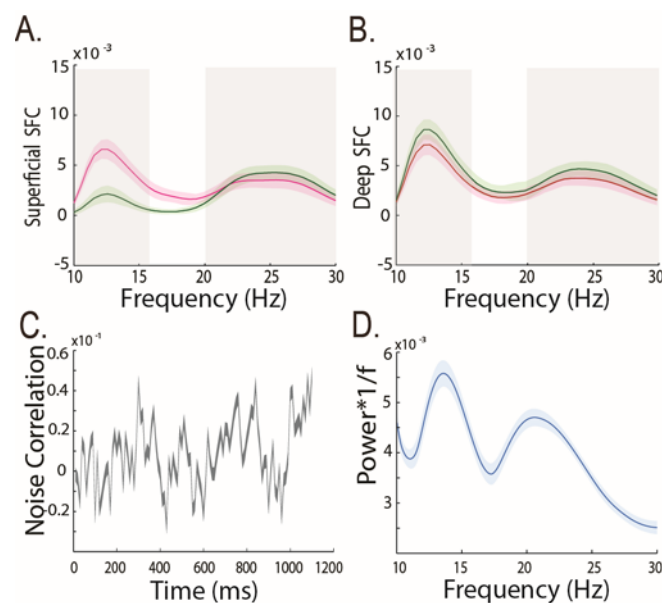
180 **Figure 3: Spike-LFP phase coupling (SFC) and noise correlations differ between**
 181 **superficial and deep layers.** (A) Distribution of SFC in gamma- and - alpha-bands
 182 for superficial and deep layers in area FEF. (B) Average SFC (mean +/- s.e. across
 183 sessions, calculated during 300ms to 1500ms following cue offset within superficial
 184 cortical layer signals. (C) Same as (B) but within deep cortical layer. (D) Average
 185 SFC (+/- s.e.) in alpha (10-16Hz, top histogram) and beta (20-30Hz, bottom
 186 histogram) for superficial (empty bars) and deep (filled bars) cortical layer signals
 187 (t-test, ***: $p < 0.001$).

188 Figure 3B-C represents the SFC applied to the same data as presented in figure S3, but
 189 separated on the bases of the attribution of the MUA to either superficial or deep cortical FEF
 190 layers. While SFC modulations are observed in the same frequencies of interest as in figure S3,
 191 i.e. in the high alpha range (10-16Hz) and the beta range (20-30Hz), clear layer differences can
 192 be observed (figure 3B-C). Specifically, within superficial layers (figure 3B), SFC is selectively
 193 enhanced in the high alpha (10-16Hz) frequency range when spatial memory is oriented towards
 194 the preferred spatial location of the recorded signals as compared to away (figure 3D, $p < 0.001$).
 195 This coincides with an enhanced high alpha power in the preferred compared to the non-
 196 preferred condition in the superficial layers (figure S4). No difference in SFC is observed in the
 197 beta frequency range, for preferred vs. non-preferred locations. In deep layers (figure 3C), SFC
 198 is enhanced in both the higher alpha and beta frequency ranges, irrespectively of whether spatial
 199 memory is oriented towards or away from the preferred spatial locations (figure 3D). This
 200 coincides, in the deep layers, with high alpha power in both the preferred and non-preferred
 201 conditions (figure S4). This result suggests distinct selective control mechanisms of correlated

202 noise, spatially selective in superficial FEF layers and non-spatially selective in deep FEF
203 layers.

204 *Modeling rhythmic variations in noise correlations*

205 In this last section, using an artificial neuronal population reproducing observed spike
206 and LFP parameters, we provide a causal and parsimonious model linking spike-field coherence
207 and noise correlations mechanisms. The input data to the model are superficial and deep LFP
208 signals generated to match the experimental observation of high alpha / gamma SFC ratio in
209 superficial cortical layers and low alpha / gamma SFC ratio in deep cortical layers (figure S5)
210 as well as FEF LFP power content as a function of preferred and non-preferred spatial memory
211 (as per figures S3 and S4). Spike data are generated such that SFC is high in the high alpha and
212 beta frequency ranges. In the model, differences in the input LFP power between the superficial
213 and deep layers in the preferred and non-preferred spatial memory conditions combined with
214 selective SFC in the high alpha and beta frequencies are sufficient to reproduce the empirical
215 SFC differences (figure 4A and 4B to be compared to figure 3B and 3C). The resultant spiking
216 population is characterized by variable noise correlations in time (figure 4C) with a marked
217 rhythmic pattern in the high alpha and beta frequency ranges (figure 4D). Importantly, these
218 rhythmic properties of neuronal noise correlations were resilient to changes in LFP power
219 outside the SFC frequency ranges. Overall, this thus points towards a local origin for the
220 reported noise correlation oscillations, implemented via selective SFC spiking mechanisms that
221 differ in their spatial selectivity between superficial and deep layers. The output of this local
222 mechanism is however further modulated by long-range influences captured by the low
223 frequency alpha and beta LFP frequency content.



224

225 **Figure 4: Modelling of rhythmic variations in noise correlations.** (A) Model
226 average SFC (mean +/- s.e.) within superficial cortical layer signals. (B) Same as
227 in (A) but within deep cortical layer signals. (C) Model example of noise correlation
228 variations as a function of trial time. (D) 1/f weighted power frequency spectrum
229 of noise correlation in time (mean +/- s.e.) presented in (C).

230 Overall, we thus propose a model that shows that the observed rhythmic variations in
231 noise correlations can be parsimoniously explained by selective SFC mechanisms in the higher
232 alpha and beta frequency ranges, the strength of which are modulated by LFP power in these
233 specific frequency bands irrespective of other frequencies.

234

235 **Discussion**

236 *Oscillations in noise correlations at multiple time scales.*

237 Here, we describe, in the prefrontal cortex, two distinct regimens of rhythmic
238 fluctuations in noise correlations, namely in the high alpha (10-16 Hz) frequency range as well
239 as in the beta (20-30Hz) frequency range. These dominate over faster fluctuations in the gamma
240 band (data not shown), as described in the primary visual cortex by ²⁶, and which have been
241 shown to coincide with variations in stimulus selectivity and enhanced gamma-band
242 synchronization. Interestingly, identical rhythmic fluctuations in noise correlations can also be
243 identified in the parietal cortex (LIP, data not shown). FEF and LIP belong to the same
244 functional network ^{28,62} and are densely interconnected ^{63,64}. It is thus not surprising that both
245 cortical areas share the same noise correlation rhythmic properties, and supports a long-range
246 origin for these rhythmic patterns (see below). Whether this noise correlations rhythms are
247 ubiquitous and extend to, for example, the primary visual cortex, or whether they are specific
248 to the parieto-frontal cortex and in tight link with the role of this functional network in
249 attentional processes remains to be explored ^{28,62,65}. Importantly, these rhythmic fluctuations in
250 noise correlations are not specific to spatial memory processes, and can be observed in simple
251 fixation or target detection tasks ⁶⁶.

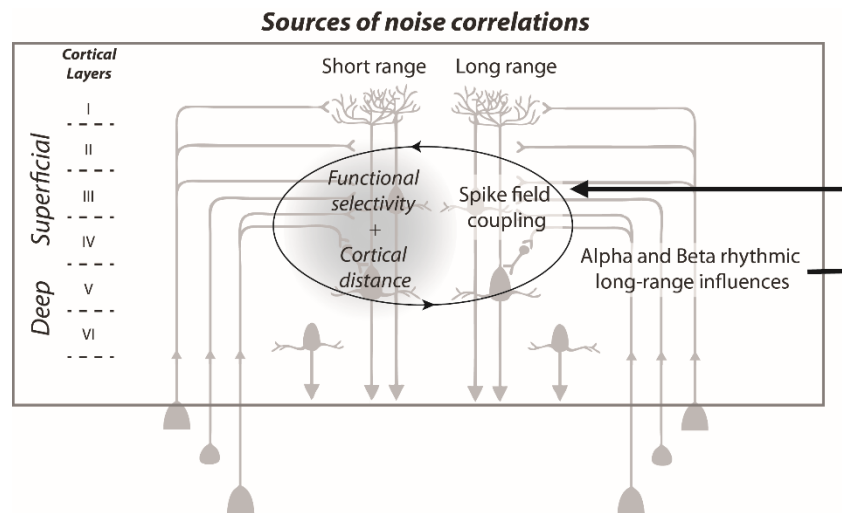
252 *Rhythmic noise correlations in neuronal population impact information capacity and* 253 *behavior.*

254 The information capacity of a population code is thought to decrease as correlated noise
255 among neurons increases ^{3,13,14,67}, thought recent studies suggest that this detrimental aspect
256 depends of noise correlation sources ^{12,68}. Accordingly, fluctuations in noise correlations levels
257 are expected to coincide with fluctuations in neuronal information. In V1, gamma-band

258 fluctuations in primary visual cortex noise correlations are associated with variations in
259 stimulus selectivity²⁶. Under the legitimate assumption of a direct relationship between
260 prefrontal neuronal population information content and subjects' behavior, a strong prediction
261 of the dependency between overall neuronal population information capacity and noise
262 correlations is a link between noise correlations and overt behavior. Here, we show that overt
263 behavioral performances co-vary with both the alpha and beta noise correlation oscillations,
264 accounting for up to 10% of the behavioral response variability. This indicates a functional role
265 for these alpha and beta oscillations in noise correlations and supports the idea that noise
266 correlation is a flexible physiological parameter that modulates overall neuronal population
267 information capacity. Recent studies show that noise correlation contributes to optimally meet
268 ongoing behavioral demands, during learning and attention⁶⁹. In a twin study, we show that
269 noise correlations vary in strength both as a function of the ongoing task as well as a function
270 of the time in the task, thus adjusting dynamically to ongoing behavioral demands⁶⁶.

271 *Cognitive rhythms and noise correlations.*

272 Alpha oscillations are consistently associated with attention, anticipation^{45,46},
273 perception⁴⁷⁻⁴⁹, and working memory⁵⁰. Beta oscillations are on the other hand consistently
274 associated with cognitive control and cognitive flexibility⁶². Gamma-oscillations reflect local
275 neuronal processes propagating in the feedforward direction⁷⁰ and spatial attention orientation
276 coincides with increased gamma oscillations^{33,71} as well as increased SFC^{72,73}. In contrast,
277 alpha⁷⁰ and beta⁶² oscillations reflect long-range processes propagating in the feedback
278 direction, and spatial attention orientation coincides with decreased alpha and beta SFC. Our
279 recordings are performed in the FEF, a cortical region which has been demonstrated to be at the
280 source of spatial attention control signals²⁷⁻³⁰. In this cortical region, rhythmic processes in
281 relation with spatial attention deployment have recently been described both in the theta^{25,74}
282 and in the lower alpha⁸³ frequencies, supporting the hypothesis that attention is an intrinsically
283 rhythmic cognitive process²⁵. The oscillations in noise correlation described here take place in
284 frequency ranges that are independent from those described in spatial attention and memory
285 studies. This suggests that they are of a different neuronal origin and correlate with neuronal
286 mechanisms that are distinct from those at play during selective spatial cognitive processes.



287

288 **Sources of noise correlations.** Noise correlations are shaped by short-range inter-
289 neuronal connectivity that depend both on cortical distance and on functional
290 selectivity (left) and by alpha and beta rhythmic long-range influences that
291 differentially impact spike LFP phase coupling in the superficial and deep cortical
292 layer.

293 **Mechanism accounting for rhythmic noise correlations.**

294 The rhythmic fluctuations in noise correlations we describe here co-exist with rhythmic
295 fluctuations of SFC in the same frequency ranges. This supports a functional link between these
296 two processes. The origin of this shared noise variability is still a subject of debate; it can arise
297 from the afferent pathways^{2,4}, from top-down signals^{75,76}, or from coherent synchronization
298 mechanisms in functional sub-networks. Our model confirms that rhythmic variations in noise
299 correlations are parsimoniously accounted for by joint long-range influences reflected in the
300 LFP alpha and beta ranges and selective local SFC mechanisms in these very same frequencies.
301 This causal link being irrespective of changes in LFP power away from these frequency ranges.
302 In other words, long-range high alpha and beta modulate the degree of synchronization between
303 local neuronal populations (figure 5, right). Confirming this observation, we show that at the
304 same time as the strength of noise correlation high alpha and beta oscillations vary as a function
305 of the ongoing task, so does SFC⁶⁶. Supporting these long-range influences on noise
306 correlations, we show that, in the absence of spatial memory signals, SFC modulation in the
307 alpha range strongly decreases in the more superficial cortical layers as compared to the deeper
308 layers. We propose that SFC coupling selectivity to specific frequency ranges is due to the
309 biophysical membrane properties of specific prefrontal cell types⁷⁷. This will need to be further
310 investigated. In addition to these long-range modulations, local recurrent connectivity also

311 affects noise correlations ¹². This results in the classical observation that shared neuronal
312 variability decreases as a function of cortical distance as well as a function of functional
313 dissimilarity between neuronal pairs (figure 5, left). The extent to which these local recurrent
314 mechanisms differ between superficial and deeper layers remains to be explored.

315 Overall, this thus leads to the strong prediction that local flexibility in noise correlations
316 as a function of behavioral demand arises from changes in long-range incoming signals in
317 specific frequency bands, namely the high alpha and beta frequencies, and acts independently
318 from other previously described neuronal processes such as spatial attention and spatial memory
319 processes. The exact source of these signals, their relation to behavioral optimization and
320 flexibility and how they interact and are integrated with other sources of variations in noise
321 correlations remain to be explored.

322

323

324

325 ***Acknowledgments***

326 S.B.H.H. was supported by ANR grant ANR-14-CE13-0005-1. C.G. was supported by the
327 French Ministère de l'Enseignement Supérieur et de la Recherche. S.B.H. was supported by
328 ANR grant ANR-11-BSV4-0011, ANR grant ANR-14-CE13-0005-1, and the LABEX
329 CORTEX (ANR-11-LABX-0042) of Université de Lyon, within the program Investissements
330 d'Avenir (ANR-11-IDEX-0007) operated by the French National Research Agency (ANR).
331 E.A. was supported by the CNRS-DGA and Fondation pour la Recherche Médicale. We thank
332 research engineer Serge Pinède for technical support and Jean-Luc Charieau and Fabrice Hérant
333 for animal care. All procedures were approved by the local animal care committee (C2EA42-
334 13-02-0401-01) in compliance with the European Community Council, Directive 2010/63/UE
335 on Animal Care.

336

337 ***Authors contributions***

338 Conceptualization, S.B.H. S.B.H.H. and C.G.; Methodology, S.B.H., S.B.H.H., C.G., E.A.,
339 C.W.; Investigation, S.B.H., S.B.H.H., C.G., E.A. and C.W.; Writing – Original Draft, S.B.H.
340 S.B.H.H. and C.G.; Writing – Review & Editing, S.B.H. S.B.H.H. and C.G.; Funding
341 Acquisition, S.B.H.; Supervision, S.B.H.

342

343 *References*

- 344 1. Bach, M. & Kruger, J. Correlated neuronal variability in monkey visual cortex revealed by
345 a multi-microelectrode. *Exp. Brain Res.* 61, (1986).
- 346 2. Zohary, E., Shadlen, M. N. & Newsome, W. T. Correlated neuronal discharge rate and its
347 implications for psychophysical performance. *Nature* 370, 140–143 (1994).
- 348 3. Averbeck, B. B., Latham, P. E. & Pouget, A. Neural correlations, population coding and
349 computation. *Nat. Rev. Neurosci.* 7, 358–366 (2006).
- 350 4. Shadlen, M. N. & Newsome, W. T. The variable discharge of cortical neurons: implications
351 for connectivity, computation, and information coding. *J. Neurosci. Off. J. Soc. Neurosci.*
352 18, 3870–3896 (1998).
- 353 5. Ecker, A. S. et al. State Dependence of Noise Correlations in Macaque Primary Visual
354 Cortex. *Neuron* 82, 235–248 (2014).
- 355 6. Goris, R. L. T., Movshon, J. A. & Simoncelli, E. P. Partitioning neuronal variability. *Nat.*
356 *Neurosci.* 17, 858–865 (2014).
- 357 7. Wimmer, K. et al. Sensory integration dynamics in a hierarchical network explains choice
358 probabilities in cortical area MT. *Nat. Commun.* 6, 6177 (2015).
- 359 8. Ben-Yishai, R., Bar-Or, R. L. & Sompolinsky, H. Theory of orientation tuning in visual
360 cortex. *Proc. Natl. Acad. Sci. U. S. A.* 92, 3844–3848 (1995).
- 361 9. Litwin-Kumar, A. & Doiron, B. Slow dynamics and high variability in balanced cortical
362 networks with clustered connections. *Nat. Neurosci.* 15, 1498–1505 (2012).
- 363 10. Ly, C., Middleton, J. W. & Doiron, B. Cellular and circuit mechanisms maintain low spike
364 co-variability and enhance population coding in somatosensory cortex. *Front. Comput.*
365 *Neurosci.* 6, 7 (2012).
- 366 11. Kanitscheider, I., Coen-Cagli, R. & Pouget, A. Origin of information-limiting noise
367 correlations. *Proc. Natl. Acad. Sci. U. S. A.* 112, E6973–6982 (2015).
- 368 12. Moreno-Bote, R. et al. Information-limiting correlations. *Nat. Neurosci.* 17, 1410 (2014).
- 369 13. Sompolinsky, H., Yoon, H., Kang, K. & Shamir, M. Population coding in neuronal systems
370 with correlated noise. *Phys. Rev. E Stat. Nonlin. Soft Matter Phys.* 64, 051904 (2001).
- 371 14. Abbott, L. F. & Dayan, P. The Effect of Correlated Variability on the Accuracy of a
372 Population Code. (1999).
- 373 15. Cohen, M. R. & Maunsell, J. H. R. Attention improves performance primarily by reducing
374 interneuronal correlations. *Nat. Neurosci.* 12, 1594–1600 (2009).
- 375 16. Gawne, T. J., Kjaer, T. W., Hertz, J. A. & Richmond, B. J. Adjacent visual cortical complex
376 cells share about 20% of their stimulus-related information. *Cereb. Cortex N. Y. N* 1991 6,
377 482–489 (1996).
- 378 17. Gawne, T. J. & Richmond, B. J. How independent are the messages carried by adjacent
379 inferior temporal cortical neurons? *J. Neurosci. Off. J. Soc. Neurosci.* 13, 2758–2771
380 (1993).
- 381 18. Gutnisky, D. A. & Dragoi, V. Adaptive coding of visual information in neural populations.
382 *Nature* 452, 220–224 (2008).
- 383 19. Huang, X. & Lisberger, S. G. Noise Correlations in Cortical Area MT and Their Potential
384 Impact on Trial-by-Trial Variation in the Direction and Speed of Smooth-Pursuit Eye
385 Movements. *J. Neurophysiol.* 101, 3012–3030 (2009).
- 386 20. Mitchell, J. F., Sundberg, K. A. & Reynolds, J. H. Spatial attention decorrelates intrinsic
387 activity fluctuations in macaque area V4. *Neuron* 63, 879–888 (2009).
- 388 21. Poort, J. & Roelfsema, P. R. Noise correlations have little influence on the coding of
389 selective attention in area V1. *Cereb. Cortex N. Y. N* 1991 19, 543–553 (2009).
- 390 22. Reich, D. S. Independent and Redundant Information in Nearby Cortical Neurons. *Science*
391 294, 2566–2568 (2001).

- 392 23. Smith, M. A. & Kohn, A. Spatial and Temporal Scales of Neuronal Correlation in Primary
393 Visual Cortex. *J. Neurosci.* 28, 12591–12603 (2008).
- 394 24. Fiebelkorn, I. C., Pinsk, M. A. & Kastner, S. The mediodorsal pulvinar coordinates the
395 macaque fronto-parietal network during rhythmic spatial attention. *Nat. Commun.* 10, 215
396 (2019).
- 397 25. Fiebelkorn, I. C., Pinsk, M. A. & Kastner, S. A Dynamic Interplay within the Frontoparietal
398 Network Underlies Rhythmic Spatial Attention. *Neuron* 99, 842-853.e8 (2018).
- 399 26. Womelsdorf, T. et al. Orientation selectivity and noise correlation in awake monkey area
400 V1 are modulated by the gamma cycle. *Proc. Natl. Acad. Sci. U. S. A.* 109, 4302 (2012).
- 401 27. Astrand, E., Ibos, G., Duhamel, J.-R. & Ben Hamed, S. Differential dynamics of spatial
402 attention, position, and color coding within the parietofrontal network. *J. Neurosci. Off. J.*
403 *Soc. Neurosci.* 35, 3174–3189 (2015).
- 404 28. Ibos, G., Duhamel, J.-R. & Ben Hamed, S. A functional hierarchy within the parietofrontal
405 network in stimulus selection and attention control. *J. Neurosci. Off. J. Soc. Neurosci.* 33,
406 8359–8369 (2013).
- 407 29. Moore, T., Armstrong, K. M. & Fallah, M. Visuomotor origins of covert spatial attention.
408 *Neuron* 40, 671–683 (2003).
- 409 30. Wardak, C., Ibos, G., Duhamel, J.-R. & Olivier, E. Contribution of the monkey frontal eye
410 field to covert visual attention. *J. Neurosci. Off. J. Soc. Neurosci.* 26, 4228–4235 (2006).
- 411 31. Meyers, E. M., Qi, X.-L. & Constantinidis, C. Incorporation of new information into
412 prefrontal cortical activity after learning working memory tasks. *Proc. Natl. Acad. Sci. U.*
413 *S. A.* 109, 4651–4656 (2012).
- 414 32. Constantinidis, C. & Klingberg, T. The neuroscience of working memory capacity and
415 training. *Nat. Rev. Neurosci.* 17, 438–449 (2016).
- 416 33. Gregoriou, G. G., Gotts, S. J., Zhou, H. & Desimone, R. High-frequency, long-range
417 coupling between prefrontal and visual cortex during attention. *Science* 324, 1207–1210
418 (2009).
- 419 34. Gregoriou, G. G., Gotts, S. J. & Desimone, R. Cell-type-specific synchronization of neural
420 activity in FEF with V4 during attention. *Neuron* 73, 581–594 (2012).
- 421 35. Armstrong, K. M., Chang, M. H. & Moore, T. Selection and maintenance of spatial
422 information by frontal eye field neurons. *J. Neurosci. Off. J. Soc. Neurosci.* 29, 15621–
423 15629 (2009).
- 424 36. Constantinidis, C. & Goldman-Rakic, P. S. Correlated discharges among putative
425 pyramidal neurons and interneurons in the primate prefrontal cortex. *J. Neurophysiol.* 88,
426 3487–3497 (2002).
- 427 37. Lee, D., Port, N. L., Kruse, W., Georgopoulos, A. P. & Neurology. Variability and
428 correlated noise in the discharge of neurons in motor and parietal areas of the primate
429 cortex. *J Neurosci* 18,1161–1170. (1998).
- 430 38. Bair, W., Zohary, E. & Newsome, W. T. Correlated firing in macaque visual area MT: time
431 scales and relationship to behavior. *J. Neurosci. Off. J. Soc. Neurosci.* 21, 1676–1697
432 (2001).
- 433 39. Dugué, L., Roberts, M. & Carrasco, M. Attention Reorients Periodically. *Curr. Biol. CB*
434 *26*, 1595–1601 (2016).
- 435 40. Fiebelkorn, I. C., Saalman, Y. B. & Kastner, S. Rhythmic sampling within and between
436 objects despite sustained attention at a cued location. *Curr. Biol. CB* 23, 2553–2558 (2013).
- 437 41. Landau, A. N. & Fries, P. Attention samples stimuli rhythmically. *Curr. Biol. CB* 22, 1000–
438 1004 (2012).
- 439 42. VanRullen, R. Visual Attention: A Rhythmic Process? *Curr. Biol.* 23, R1110–R1112
440 (2013).

- 441 43. Corentin, G. et al. Prefrontal attentional saccades explore space at an alpha rhythm. *bioRxiv*
442 637975 (2019).
- 443 44. Astrand, E., Wardak, C., Baraduc, P. & Ben Hamed, S. Direct Two-Dimensional Access to
444 the Spatial Location of Covert Attention in Macaque Prefrontal Cortex. *Curr. Biol.* CB 26,
445 1699–1704 (2016).
- 446 45. Thut, G., Nietzel, A., Brandt, S. A. & Pascual-Leone, A. Alpha-band
447 electroencephalographic activity over occipital cortex indexes visuospatial attention bias
448 and predicts visual target detection. *J. Neurosci. Off. J. Soc. Neurosci.* 26, 9494–9502
449 (2006).
- 450 46. Rihs, T. A., Michel, C. M. & Thut, G. A bias for posterior alpha-band power suppression
451 versus enhancement during shifting versus maintenance of spatial attention. *NeuroImage*
452 44, 190–199 (2009).
- 453 47. Varela, F. J., Toro, A., John, E. R. & Schwartz, E. L. Perceptual framing and cortical alpha
454 rhythm. *Neuropsychologia* 19, 675–686 (1981).
- 455 48. Mathewson, K. E., Gratton, G., Fabiani, M., Beck, D. M. & Ro, T. To See or Not to See:
456 Prestimulus α Phase Predicts Visual Awareness. *J. Neurosci.* 29, 2725–2732 (2009).
- 457 49. Busch, N. A. & VanRullen, R. Spontaneous EEG oscillations reveal periodic sampling of
458 visual attention. *Proc. Natl. Acad. Sci. U. S. A.* 107, 16048–16053 (2010).
- 459 50. Klimesch, W. EEG-alpha rhythms and memory processes. *Int. J. Psychophysiol. Off. J. Int.*
460 *Organ. Psychophysiol.* 26, 319–340 (1997).
- 461 51. Bruce, C. J. & Goldberg, M. E. Primate frontal eye fields: I. Single neurons discharging
462 before saccades. *J. Neurophysiol.* 53(3), 603–635 (1985).
- 463 52. Segraves, M. A. & Goldberg, M. E. Functional properties of corticotectal neurons in the
464 monkey's frontal eye field. *J. Neurophysiol.* 58, 1387–1419 (1987).
- 465 53. Schall, J. D. Neuronal activity related to visually guided saccades in the frontal eye fields
466 of rhesus monkeys: comparison with supplementary eye fields. *J. Neurophysiol.* 66, 559–
467 579 (1991).
- 468 54. Schall, J. D. & Hanes, D. P. Neural basis of saccade target selection in frontal eye field
469 during visual search. *Nature* 366, 467–469 (1993).
- 470 55. Schall, J. D., Hanes, D. P., Thompson, K. G. & King, D. J. Saccade target selection in
471 frontal eye field of macaque. I. Visual and premovement activation. *J. Neurosci. Off. J. Soc.*
472 *Neurosci.* 15, 6905–6918 (1995).
- 473 56. Schall, J. D. & Thompson, K. G. Neural selection and control of visually guided eye
474 movements. *Annu. Rev. Neurosci.* 22, 241–259 (1999).
- 475 57. Pouget, P. et al. Visual and motor connectivity and the distribution of calcium-binding
476 proteins in macaque frontal eye field: implications for saccade target selection. *Front.*
477 *Neuroanat.* 3, 2 (2009).
- 478 58. Fries, W. Cortical projections to the superior colliculus in the macaque monkey: a
479 retrograde study using horseradish peroxidase. *J. Comp. Neurol.* 230, 55–76 (1984).
- 480 59. Leichnetz, G. R. & Goldberg, M. E. Higher centers concerned with eye movement and
481 visual attention: cerebral cortex and thalamus. *Rev. Oculomot. Res.* 2, 365–429 (1988).
- 482 60. Sommer, M. A. & Wurtz, R. H. Composition and Topographic Organization of Signals Sent
483 From the Frontal Eye Field to the Superior Colliculus. *J. Neurophysiol.* 83, 1979–2001
484 (2000).
- 485 61. Buffalo, E. A., Fries, P., Landman, R., Buschman, T. J. & Desimone, R. Laminar
486 differences in gamma and alpha coherence in the ventral stream. *Proc. Natl. Acad. Sci. U.*
487 *S. A.* 108, 11262–11267 (2011).
- 488 62. Buschman, T. J. & Miller, E. K. Top-down versus bottom-up control of attention in the
489 prefrontal and posterior parietal cortices. *Science* 315, 1860–1862 (2007).

- 490 63. Cavada, C. & Goldman-Rakic, P. S. Posterior parietal cortex in rhesus monkey: II.
491 Evidence for segregated corticocortical networks linking sensory and limbic areas with the
492 frontal lobe. *J. Comp. Neurol.* 287, 422–445 (1989).
- 493 64. Stanton, G. B., Bruce, C. J. & Goldberg, M. E. Topography of projections to posterior
494 cortical areas from the macaque frontal eye fields. *J. Comp. Neurol.* 353, 291–305 (1995).
- 495 65. Corbetta, M. & Shulman, G. L. Control of goal-directed and stimulus-driven attention in
496 the brain. *Nat. Rev. Neurosci.* 3, 201–215 (2002).
- 497 66. Hassen, S. B. H., Gaillard, C., Astrand, E., Wardak, C. & Hamed, S. B. Interneuronal
498 correlations dynamically adjust to task demands at multiple time-scales. *bioRxiv* 547802
499 (2019).
- 500 67. Tremblay, S., Pieper, F., Sachs, A. & Martinez-Trujillo, J. Attentional filtering of visual
501 information by neuronal ensembles in the primate lateral prefrontal cortex. *Neuron* 85, 202–
502 215 (2015).
- 503 68. Kohn, A., Coen-Cagli, R., Kanitscheider, I. & Pouget, A. Correlations and Neuronal
504 Population Information. *Annu. Rev. Neurosci.* 39, 237–256 (2016).
- 505 69. Ni, A. M., Ruff, D. A., Alberts, J. J., Symmonds, J. & Cohen, M. R. Learning and attention
506 reveal a general relationship between population activity and behavior. *Science* 359, 463–
507 465 (2018).
- 508 70. van Kerkoerle, T. et al. Alpha and gamma oscillations characterize feedback and
509 feedforward processing in monkey visual cortex. *Proc. Natl. Acad. Sci. U. S. A.* 111,
510 14332–14341 (2014).
- 511 71. Fries, P., Reynolds, J. H., Rorie, A. E. & Desimone, R. Modulation of Oscillatory Neuronal
512 Synchronization by Selective Visual Attention. *Science* 291, 1560–1563 (2001).
- 513 72. Chalk, M. et al. Attention Reduces Stimulus-Driven Gamma Frequency Oscillations and
514 Spike Field Coherence in V1. *Neuron* 66, 114 (2010).
- 515 73. Engel, A. K., Fries, P. & Singer, W. Dynamic predictions: oscillations and synchrony in
516 top-down processing. *Nat. Rev. Neurosci.* 2, 704–716 (2001).
- 517 74. Spyropoulos, G., Bosman, C. A. & Fries, P. A theta rhythm in macaque visual cortex and
518 its attentional modulation. *Proc. Natl. Acad. Sci. U. S. A.* 115, E5614–E5623 (2018).
- 519 75. Ecker, A. S. et al. Decorrelated Neuronal Firing in Cortical Microcircuits. *Science* 327,
520 584–587 (2010).
- 521 76. Nienborg, H. & Cumming, B. Correlations between the activity of sensory neurons and
522 behavior: how much do they tell us about a neuron’s causality? *Curr. Opin. Neurobiol.* 20,
523 376–381 (2010).
- 524 77. Trainito, C., von Nicolai, C., Miller, E. K. & Siegel, M. Extracellular Spike Waveform
525 Dissociates Four Functionally Distinct Cell Classes in Primate Cortex. *Curr. Biol.* 29,
526 R871–R873 (2019).
- 527 78. Oostenveld, R., Fries, P., Maris, E. & Schoffelen, J.-M. FieldTrip: Open Source Software
528 for Advanced Analysis of MEG, EEG, and Invasive Electrophysiological Data. *Intell*
529 *Neurosci.* 2011, 1:1–1:9 (2011).
- 530 79. Grinsted, A., Moore, J. C. & Jevrejeva, S. Application of the cross wavelet transform and
531 wavelet coherence to geophysical time series. *Nonlinear Process. Geophys.* 11, 561–566
532 (2004).
- 533 80. Buffalo, E. A., Fries, P., Landman, R., Buschman, T. J. & Desimone, R. Laminar
534 differences in gamma and alpha coherence in the ventral stream. *Proc. Natl. Acad. Sci. U.*
535 *S. A.* 108, 11262–11267 (2011).
- 536 81. Cohen, J. Y., Pouget, P., Heitz, R. P., Woodman, G. F. & Schall, J. D. Biophysical support
537 for functionally distinct cell types in the frontal eye field. *J. Neurophysiol.* 101, 912–916
538 (2009).

- 539 82. Fiebelkorn, I. C. et al. Cortical cross-frequency coupling predicts perceptual outcomes.
540 NeuroImage 69, 126–137 (2013).
- 541 83. Gaillard C., Ben Hadj Hassen S., Di Bello F., Bihan-Poudec Y., VanRullen R., Ben Hamed
542 S. Prefrontal attentional saccades explore space at an alpha rhythm. bioRxiv. doi:
543 <https://doi.org/10.1101/637975> (2019)
544
545

546 **Supplementary material and methods**

547 **Material and methods**

548 **Ethical statement**

549 All procedures were in compliance with the guidelines of European Community on
550 animal care (Directive 2010/63/UE of the European Parliament and the Council of 22
551 September 2010 on the protection of animals used for scientific purposes) and authorized by
552 the French Committee on the Ethics of Experiments in Animals (C2EA) CELYNE registered
553 at the national level as C2EA number 42 (protocole C2EA42-13-02-0401-01).

554 **Surgical procedure:**

555 As in⁴⁴, two male rhesus monkeys (*Macaca mulatta*) weighing between 6-8 kg
556 underwent a unique surgery during which they were implanted with two MRI compatible PEEK
557 recording chambers placed over the left and the right FEF hemispheres respectively (figure 1A),
558 as well as a head fixation post. Gas anesthesia was carried out using Vet-Flurane, 0.5 – 2%
559 (Isoflurane 100%) following an induction with Zolétil 100 (Tiletamine at 50mg/ml, 15mg/kg
560 and Zolazepam, at 50mg/ml, 15mg/kg). Post-surgery pain was controlled with a morphine pain-
561 killer (Buprecare, buprenorphine at 0.3mg/ml, 0.01mg/kg), 3 injections at 6 hours interval (first
562 injection at the beginning of the surgery) and a full antibiotic coverage was provided with
563 Baytril 5% (a long action large spectrum antibiotic, Enrofloxacin 0.5mg/ml) at 2.5mg/kg, one
564 injection during the surgery and thereafter one each day during 10 days. A 0.6mm isomorphic
565 anatomical MRI scan was acquired post surgically on a 1.5T Siemens Sonata MRI scanner,
566 while a high-contrast oil filled grid (mesh of holes at a resolution of 1mmx1mm) was placed in
567 each recording chamber, in the same orientation as the final recording grid. This allowed a
568 precise localization of the arcuate sulcus and surrounding gray matter underneath each of the
569 recording chambers. The FEF was defined as the anterior bank of the arcuate sulcus and we
570 specifically targeted those sites in which a significant visual and/or oculomotor activity was
571 observed during a memory guided saccade task at 10 to 15° of eccentricity from the fixation
572 point (figure 1A). In order to maximize task-related neuronal information at each of the 24-
573 contacts of the recording probes, we only recorded from sites with task-related activity observed
574 continuously over at least 3 mm of depth.

575

576 **Behavioral task:**

577 During a given experimental session, the monkeys were placed in front of a computer
578 screen (1920x1200 pixels and a refresh rate of 60 Hz) with their head fixed. Their water intake
579 was controlled so that their initial daily intake was covered by their performance in the task, on
580 a trial by trial basis. This quantity was complemented as follows. On good performance
581 sessions, monkeys received fruit and water complements. On bad performance sessions, water
582 complements were provided at a distance from the end of the session. During a *Memory-guided*
583 *saccade Task* (figure 1B): A red fixation cross ($0.7 \times 0.7^\circ$) appeared in the center of the screen
584 and the monkeys were required to hold fixation for 500 msec, within a fixation window of
585 $1.5 \times 1.5^\circ$. A square green cue ($0.28 \times 0.28^\circ$) was then flashed for 100ms at one of four possible
586 locations ($(10^\circ, 10^\circ)$, $(-10^\circ, 10^\circ)$, $(-10^\circ, -10^\circ)$ and $(10^\circ, -10^\circ)$). The monkeys had to continue
587 maintain fixation on the central fixation point for another 700–1900 ms until the fixation point
588 disappeared. The monkeys were then required to make a saccade towards the memorized
589 location of the cue within 500-800ms from fixation point disappearance, and a spatial tolerance
590 of $4^\circ \times 4^\circ$. On success, a target, identical to the cue was presented at the cued location and the
591 monkeys were required to fixate it and detect a change in its color by a bar release within 150-
592 800 ms from color change. Success in all of these successive requirements conditioned reward
593 delivery.

594 **Neural recordings:**

595 On each session, bilateral simultaneous recordings in the two FEFs were carried out
596 using two 24- contact Plexon U-probes. The contacts had an interspacing distance of 250 μm .
597 Neural data was acquired with the Plexon Omniplex® neuronal data acquisition system. The
598 data was amplified 400 times and digitized at 40,000 Hz. The MUA neuronal data was high-
599 pass filtered at 300 Hz. The LFP neuronal data was filtered between 0.5 and 300 Hz. In the
600 present paper, all analyses are performed on the multi-unit activity recorded on each of the 48
601 recording contacts. A threshold defining the multi-unit activity was applied independently for
602 each recording contact and before the actual task-related recordings started. All further analyses
603 of the data were performed in Matlab™ and using FieldTrip⁷⁸ and the Wavelet Coherence
604 Matlab Toolbox⁷⁹, both open source Matlab™ toolboxes.

605 **Data Analysis**

606 **Data preprocessing.** Overall, MUA recordings were collected from 48 recording
607 channels on 26 independent recording sessions (13 for M1 and 13 for M2). We excluded from
608 subsequent analyses all channels with less than 5 spikes per seconds. For each session, we
609 identified the task-related channels based on a statistical change (one-way ANOVA, $p < 0.05$) in
610 the MUA neuronal activity in the memory-guided saccade task, in response to either cue
611 presentation ([0 400] ms after cue onset) against a pre-cue baseline ([-100 0] ms relative to cue
612 onset), or to saccade execution go signal and to saccade execution (i.e. fixation point off, [0 400]
613 ms after go signal) against a pre-go signal baseline ([-100 0] ms relative to go signal),
614 irrespective of the spatial configuration of the trial. In total, 671 channels were retained for
615 further analyses out of 1248 channels.

616
617 **Distance between recording sites.** For each electrode, pairs of MUA recordings were
618 classified along four possible distance categories: D1, spacing of 250 μm ; D2, spacing of 500
619 μm ; D3, spacing of 750 μm and D4, spacing of 1mm. These distances are an indirect proxy to
620 actual cortical distance, as the recordings were performed tangentially to cortical surface, i.e.
621 more or less parallel to sulcal surface.

622 **MUA spatial selectivity.** FEF neurons are characterized by a strong visual, saccadic,
623 spatial memory and spatial attention selectivity^{27,28,51}. We used a one-way ANOVA ($p < 0.05$)
624 to identify the spatially selective channels in response to cue presentation ([0 400] ms following
625 cue onset) and to the saccade execution go signal ([0 400] ms following go signal). Post-hoc t-
626 tests served to further order, for each channels, the neuron's response in each visual quadrant
627 from preferred (p1), to least preferred (p4). By convention, positive modulations were
628 considered as preferred and negative modulations as least preferred. For example, in a given
629 session, the MUA signal recorded on channel 1 of a probe placed in the left FEF, could have as
630 best preferred position p1 the upper right quadrant, the next best preferred position p2 the lower
631 right quadrant, the next preferred position p3 the upper left quadrant and the least preferred
632 position p4 the lower left quadrant. The MUA signal recorded on channel 14 of this same probe,
633 could have as best preferred position p1 the lower right quadrant, the next best preferred
634 position p2 the upper right quadrant, the next preferred position p3 the lower left quadrant and
635 the least preferred position p4 the upper left quadrant. Positions with no significant modulation
636 in any task epoch were labeled as p0 (no selectivity for this position). Once this was done, for
637 each electrode, pairs of MUA recordings were classified along two possible functional
638 categories: pairs with the same spatial selectivity (SSS pairs, sharing the same p1) and pairs
639 with different spatial selectivity (DSS pairs, such that the p1 of one MUA is a p0 for the other

640 MUA). For the sake of clarity, we do not consider partial spatial selectivity pairs (such that the
641 p1 of one MUA is a non-preferred, p2, p3 or p4 for the other MUA).

642 ***MUA layer attribution.*** As stated above, our recordings are not tangential to cortical
643 surface. As a proxy to attribute a given recording channel to upper or lower cortical layers we
644 proceeded as follows. For each electrode and each channel, we estimated, at the time of cue
645 onset in the memory-guided saccade task (100ms-500ms from cue onset), the SFC in the alpha
646 range (6 to 16 Hz) and the gamma range (40 to 60 Hz). Based on previous literature⁸⁰, we used
647 the ratio between the alpha and gamma spike field-coherence as a proxy to assign the considered
648 LFP signals to a deep cortical layer site (high alpha / gamma spike-field coherence ratio) or to
649 a superficial cortical layer site (low alpha / gamma SFC ratio). We also categorized MUA
650 signals into visual, visuo-motor and motor categories, as in⁸¹. Briefly, average firing rates were
651 computed in 3 epochs: [-100 0] ms before cue onset (baseline), [0 200] ms after cue onset
652 (visual), and [0 200] ms before saccade onset (movement). Neurons with activity statistically
653 significantly different from the baseline (Wilcoxon rank-sum test, $P < 0.05$) after cue onset
654 were categorized as visual. Neurons with activity statistically significantly different from the
655 baseline (Wilcoxon rank-sum test, $P < 0.05$) before saccade onset were categorized as
656 oculomotor. Neurons that were active in both epochs were categorized as visuo-movement
657 neurons. The LFP categorization along the alpha to gamma SFC ratio strongly coincided with
658 the classification of the MUA signals into purely visual sites (low alpha and gamma SFC ratio,
659 input FEF layers) and visuo-motor sites (high alpha and gamma SFC ratio, output FEF layers,
660 figure 3).

661 ***Oscillations in noise correlations.*** To measure oscillatory patterns in the noise
662 correlation time-series data, we computed for each session (N=12) noise correlations over time
663 (over successive 200ms intervals, sliding by 10ms, running from 300ms to 1500ms following
664 cue offset). Specifically, for each channel i , and each trial k , the average neuronal response $r_i(k)$
665 for the 200 ms interval was calculated and z-score normalized into $z_i(k)$, where $z_i(k) = r_i(k) -$
666 μ_i / std_i and μ_i and std_i respectively correspond to the mean firing rate and standard deviation
667 around this mean during the interval of interest of the channel of interest i . This z-score
668 normalization allows to capture the changes in neuronal response variability independently of
669 changes in mean firing rates. Noise correlations between pairs of MUA signals during the
670 interval of interest were then defined as the Pearson correlation coefficient between the z-scored
671 individual trial neuronal responses of each MUA signal over all trials. Only positive significant
672 noise correlations are considered, unless stated otherwise. In any given recording session, noise

673 correlations were calculated between MUA signals recorded from the same electrode, thus
674 specifically targeting intra-cortical correlations. Once noise correlation is calculated over time
675 a wavelet transform⁷⁸ was then applied on each session's noise correlation time series. To
676 control that these temporal noise correlation oscillations cannot be attributed to changes in
677 spiking activity, a wavelet analysis was also run onto MUA time series data (not shown).

678 ***Modulation of behavioral performance by alpha and beta noise correlation phase.*** To
679 quantify the effect of noise correlation oscillations onto behavioral performance, we used a
680 complex wavelet transform analysis (Fieldtrip, Oostenveld et al. 2011) to compute, for each
681 session, in the noise correlations, the phase of the frequencies of interest (alpha / beta) following
682 cue offset. For each session, we identified hit and miss trials falling at zero phase of the
683 frequency of interest ($\pm \pi / 140$) with respect to target presentation. Hit rates (HR) were
684 computed for this zero phase bin. We then shifted this phase window by $\pi / 70$ steps and
685 recalculated the HR, repeating this procedure to generate phase-detection HR functions, across
686 all phases, for each frequency of interest⁸². For each session, the phase bin for which hit rate
687 was maximal was considered as the optimal phase. The effect of a given frequency (alpha or
688 beta) onto behavior corresponds to the difference between HR at this optimal phase and HR at
689 the anti-optimal phase (optimal phase + π). To test for statistical significance, observed hit/miss
690 phases were randomized across trials so as to shuffle the temporal relationship between phases
691 and behavioral performance. This procedure was repeated 1000 times. 95% CI was then
692 computed and compared to the observed behavioral data.

693 ***Spikes-LFP PPC.*** For each selected channel, spikes-LFP phase coupling spectra (SCF)
694 were calculated between the spiking activity obtained in one channel and the LFP activity from
695 the next adjacent channel in the time interval running from 300ms to 1500ms following cue
696 offset. We used a single Hanning taper and applied convolution transform to the Hanning-
697 tapered trials. We equalized the number of trials for all conditions so as to prevent any bias that
698 could be introduced by unequal numbers of trials. We used a 4 cycles length per frequency. The
699 memory guided saccade task is known to involve spatial processes during the cue to target
700 interval that bias spike field coherence. Thus, spikes-LFP phase coupling was measured
701 separately for trials in which the cued location matched the preferred spatial location of the
702 channel and trials in which the cued location did not match the preferred spatial location of the
703 channel. Statistics were computed across channels x sessions, using a non-parametric Friedman
704 test.

705 ***Model.*** The objective of this model is to test whether rhythmic variations in noise
706 correlations can parsimoniously be explained by joint long-range influences reflected in the

707 LFP alpha and beta ranges and selective local spike-LFP phase coupling mechanisms in these
708 same frequencies. This was investigated through synthetic neuronal population activities the
709 main features of which were parsimoniously driven by FEF recorded data as follows.
710 Spikes/LFPs signals were generated to create a 200 channels X 100 trials X 1000 ms, structure.
711 LFP signals were constructed from a noise frequency component following a 1/f
712 power/frequency law, and a signal component ranging from 10Hz to 60Hz. To mimic our
713 empirical data (figure S3B), superficial LFPs to a preferred spatial memory location were
714 enriched in alpha power. Spiking activities were composed of a noise component (spikes being
715 extracted from a random binary process) and a component locked to LFP alpha (6-16Hz) and
716 beta (20-30Hz) frequency phases, thus resulting in high spikes-LFP phase coupling in these
717 specific frequencies. The strength of the SFC in each of these frequency ranges was
718 manipulated to reproduce the laminar differences observed experimentally between superficial
719 and deep cortical layer. Gamma (40-60Hz) SFC was also enhanced in the superficial FEF layers
720 to match our empirical data as well as previous reports from other cortical regions⁸⁰. It is to be
721 noted that, by definition, the strength of SFC at a specific frequency is exclusively modulated
722 by the LFP power in the same frequency range. In other words, LFP frequencies that are not
723 phase locked to the spiking activity do not contribute to the SFC measure. This can easily be
724 modeled (data not shown). Last, the functional selectivity of the synthetic channels (preferred/
725 non preferred) was mimicked by a 15% increase in firing rate in the preferred condition, while
726 the non-preferred condition remained unchanged, this for both superficial and deep channels.
727 Frequency and phase analyses were performed using Wavelet Transform Analyzes based on
728 the Wavelet Coherence Matlab Toolbox, SFC analyzes were performed using adapted Fieldtrip
729 toolbox functions (<http://fieldtriptoolbox.org>). The outcome of this phase-phase coupling
730 analysis is independent of instantaneous spiking rates.

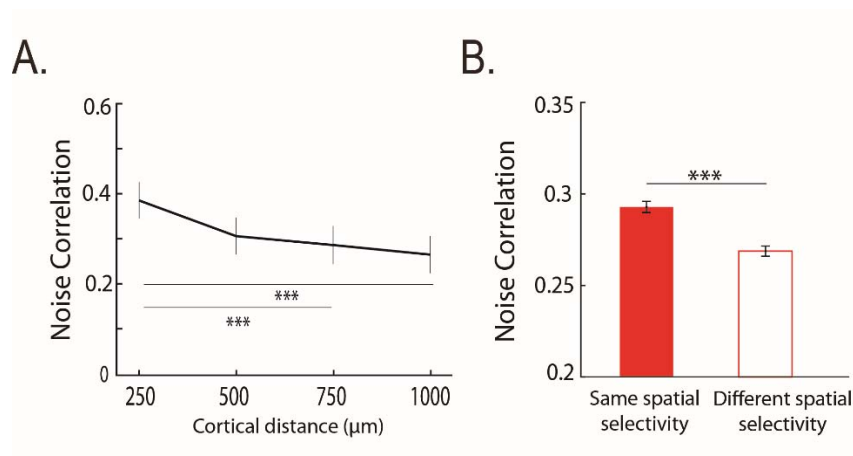
731

732

733

734 **Supplementary figures**

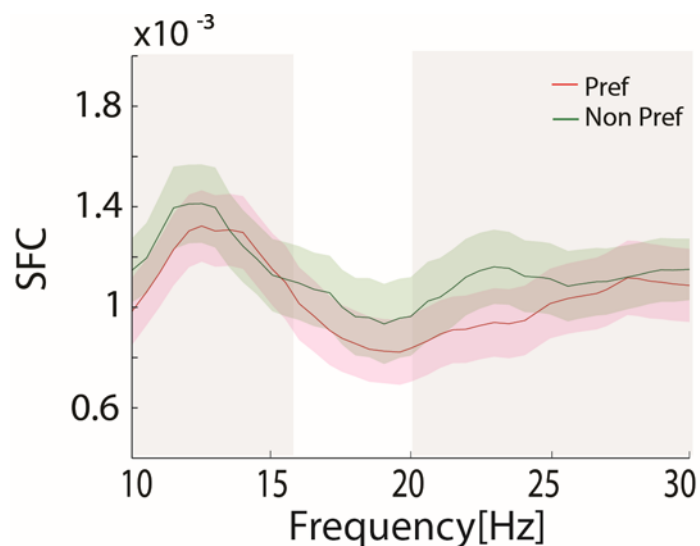
735



736

737 **Figure S1:** (A) *Noise correlations as a function of cortical distance.* Average noise correlations
738 (mean +/- s.e.) across sessions, from 300 ms to 500ms after eye fixation onset, as a function of
739 distance between pairs of channels: 250μm; 500μm; 750μm; 1000μm. (B) *Noise correlations*
740 *as a function of spatial selectivity.* Average noise correlations (mean +/- s.e.) across sessions
741 from 300ms to 500ms after eye fixation onset, as a function of whether noise correlations are
742 calculated over signals sharing the same spatial selectivity (full bars) or not (empty bars). Stars
743 indicate statistical significance following a two-way ANOVA and ranksum post-hoc tests;
744 *p<0.05; **p<0.01; ***p<0.001.

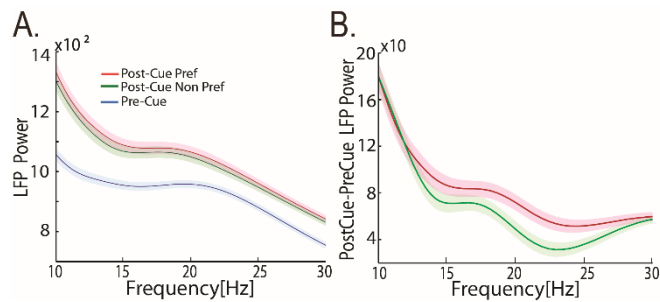
745



746

747 **Figure S2:** Average spikes-LFP phase coupling (mean +/- s.e.) across sessions, calculated
748 during 300ms to 1500ms following cue offset as a function of preferred (red line) and non-
749 preferred (green line) position.

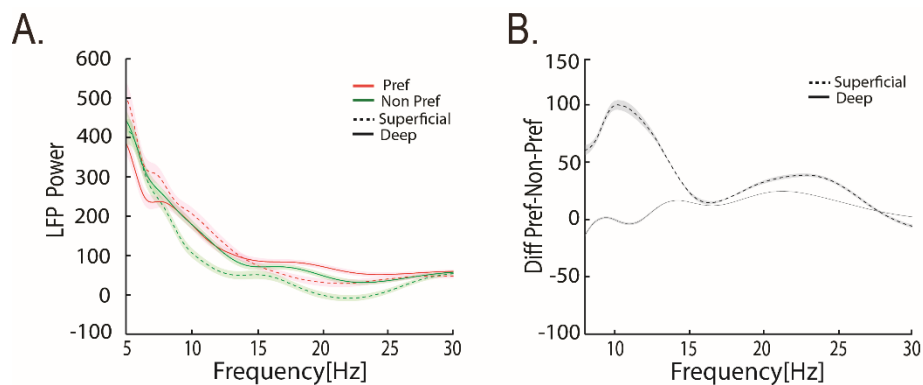
750



751

752 **Figure S3:** (A) Average of LFP power (mean \pm s.e.) across sessions, during pre-cue epoch
 753 (blue), post-cue epoch for the preferred position (red) and non-preferred position (green). (B)
 754 Difference of LFP power between post-cue preferred and non-preferred conditions for preferred
 755 (red) and non-preferred condition (green).

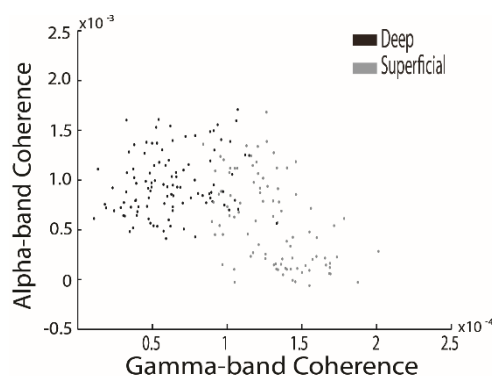
756



757

758 **Figure S4:** (A) Average of LFP power (mean \pm s.e.) across sessions, during post-cue epoch,
 759 for preferred position (red) and non-preferred position (green), in the superficial (dashed lines)
 760 and deep layers (continuous lines), relative to LFP power in pre-cue epoch. (B) Difference of
 761 LFP power between post-cue preferred and non-preferred conditions for superficial (dashed
 762 lines) and deep layers (continuous lines).

763



764

765 **Figure S5:** Model distribution of spikes-LFP phase coupling in gamma- and - alpha-bands for
 766 superficial and deep layers.

767